SCIENTIFIC REPORTS

OPEN

SUBJECT AREAS:
MECHANISMS OF DISEASE
IMAGING
BIOCHEMICAL ASSAYS
LIPIDOMICS

Received
24 June 2013

Accepted
29 October 2013

Published
20 November 2013

Correspondence and requests for materials should be addressed to N.G.-I. (naokog@tmu.ac.jp)

# Lipidomics analysis revealed the phospholipid compositional changes in muscle by chronic exercise and high-fat diet

Naoko Goto-Inoue[1,2], Kenichiro Yamada[1], Akiko Inagaki[1], Yasuro Furuichi[1], Shinya Ogino[1], Yasuko Manabe[1], Mitsutoshi Setou[2] & Nobuharu L. Fujii[1]

[1]Department of Health Promotion Sciences, Graduate School of Human Health Sciences, Tokyo Metropolitan University, 1-1, Minami-Osawa, Hachioji, Tokyo, 192-0397, Japan, [2]Department of Cell Biology and Anatomy, Hamamatsu University School of Medicine, 1-20-1, Handayama, Higashi-ku, Hamamatsu, Shizuoka, 431-3192, Japan.

**Although it is clear that lipids are responsible for insulin resistance, it is poorly understood what types of lipids are involved. In this study, we verified the characteristic lipid species in skeletal muscle of a chronic exercise training model and a high-fat induced-obesity model. Three different lipidomics analyses revealed phospholipid qualitative changes. As a result, linoleic acid-containing phosphatidylcholine and sphingomyelin and docosahexanoic acid-containing phosphatidylcholine were characterized as chronic exercise training-induced lipids. On the contrary, arachidonic acid-containing phosphatidylcholines, phosphatidylethanolamines, and phosphatidylinositol were characterized as high-fat diet-induced lipids. In addition, minor sphingomyelin, which has long-chain fatty acids, was identified as a high-fat diet-specific lipid. This is the first report to reveal compositional changes in phospholipid molecular species in chronic exercise and high-fat-diet-induced insulin-resistant models. Due to their influence on cell permeability and receptor stability at the cell membrane, these molecules may contribute to the mechanisms underlying insulin sensitivity and several metabolic disorders.**

Lipids in skeletal muscle play a fundamental role as an energy source in both normal muscle metabolism and disease states[1]. Excess accumulation of lipid in skeletal muscle is associated with several metabolic disorders, including obesity, insulin resistance, and type 2 diabetes[2]. Several studies have demonstrated strong associations between high triacylglycerol (TAG) content and enhanced skeletal muscle insulin resistance in obesity[3]. TAG content is a far stronger predictor of muscle insulin resistance than circulating fatty acids[4]. Nonetheless, highly insulin-sensitive, endurance-trained athletes also exhibit high TAG content similar to that observed in insulin-resistant obese patients. To account for this discrepancy of the so-called "athlete's paradox", a number of studies have been conducted to identify additional lipid markers in exercise training and obesity models. Among such biomarker candidates are diacylglycerol (DAG) and free ceramides, both of which have been determined to be insulin-resistant responsible lipotoxic molecules. Liu and co-workers reported that the reduction in DAG is evidence of this paradox, namely, diacylglycerol acyltransferase (DGAT1) is an important factor in the athlete's paradox, in that higher DGAT1 activity in the athlete leads to TAG accumulation[5]. A reduction in ceramide has also been revealed in another chronic exercise model[6]. In obesity, it is thought that an increased supply of fatty acids leads to the accumulation of lipotoxic fatty acid derivatives such as DAG and ceramide[7]. However, this result is controversial, because in a study by Amati and colleagues[8] using different experimental conditions, decreased amounts of DAG were reported in obese subjects.

Almost all previously reported investigations of chronic exercise training and/or high-fat diet models have focused on TAG, DAG, and ceramide contents. One study involved phospholipid analyses using thin-layer chromatography (TLC) in a 6-week endurance training regimen[9], but their detailed molecular species profiles was not examined. Phospholipids are major lipid species. These lipid species consist of the molecular layer of the cell membrane, and a phospholipid monolayer surrounds the neutral core of the lipid droplet in muscle; thus, lipid accumulation is attributed to these lipids. Moreover, DAG can also be converted into phospholipids by diacylglycerol kinases[4], and these phospholipids were shown to be associated with inflammation[3]. Remodeled

fatty acid contents of phospholipids are influenced in cell permeability and receptor stability on the cell membrane. A recent analysis revealed that phospholipid distribution differs among cell types, leading to different types of signal transduction within cells[10]. Also fascinating was the identification of a phosphatidylcholine molecular species as an important endogenous ligand for peroxisome proliferator-activated receptor α in the liver[11]. These results have fuelled speculation that phospholipids play an important role in the regulation of insulin sensitivity, and therefore compositional changes in these lipids should be analyzed. To detect and identify characteristic phospholipids, we focused on two types of rat model, namely, rats exposed to chronic exercise training (Training) and those fed a high-fat diet (HFD). Training rats were subjected to 6-week treadmill training, and this group showed increased insulin sensitivity[12]. The HFD rats were subjected to 12 weeks of feeding on a 60% high-fat diet; this group showed insulin-resistant and tendency of obese. In this report, we performed three different lipidomics approaches, thin-layer chromatography (TLC), imaging mass spectrometry (IMS), and their combined TLC-Blot-MALDI-IMS method to those models. IMS is an imaging approach that enables the visualization of a wide range of biomolecules such as lipids[13–16], glycolipids[17–19], and proteins[20,21], as well as nutrients[22,23]. This imaging modality is expected to be a suitable tool for investigating the pathologic conditions of different muscle groups, because it enables the visualization of individual lipid molecules on tissue sections. Our previous study using IMS successfully demonstrated PC changes during acute contraction at the molecular-species level[24]. In addition, we combined IMS technologies with TLC, in a method we designated as TLC-Blot-MALDI-IMS[25,26]. The method can achieve high sensitivity[27], and our previous studies validated the linearity and reproducibility of this method[26]. With IMS alone, it remains difficult to quantify ionized biomolecules because 1) multiple molecules can overlap within a single *m/z* value, and 2) the ionization efficiency differs depending on the respective structures of the molecules analyzed[28]. Fortunately in TLC-Blot-MALDI-IMS, each lipid species can be purified from background compounds or other intermediates by TLC separation, as such intermediates suppress the ionization of lipids. In the absence of these intermediate molecules, it is possible to conduct quantitative analyses of molecules on a PVDF membrane[29]. The aims of the present study were to identify and characterize lipid biomarkers specific for chronic exercise and/or high-fat-diet model, and to reveal what types of lipids are involved in insulin sensitivity/resistance in skeletal muscle.

## Results

**Subject characteristics.** Six weeks of chronic exercise training and 12 weeks of a high-fat diet did not severely affect the body weight compared to that of either Sedentary rats or rats fed a diet with a normal fat content (Fig. 1A and Table 1). To the contrary, the blood glucose level at starvation was significantly decreased in the Training group and increased in the HFD rats, compared to the control for each (Fig. 1A and Table 1). As shown in Figure 1B, blood glucose levels in the Training rats were significantly lower than those in the Sedentary rats at 15 and 60 min after glucose injection (Fig. 1B), and

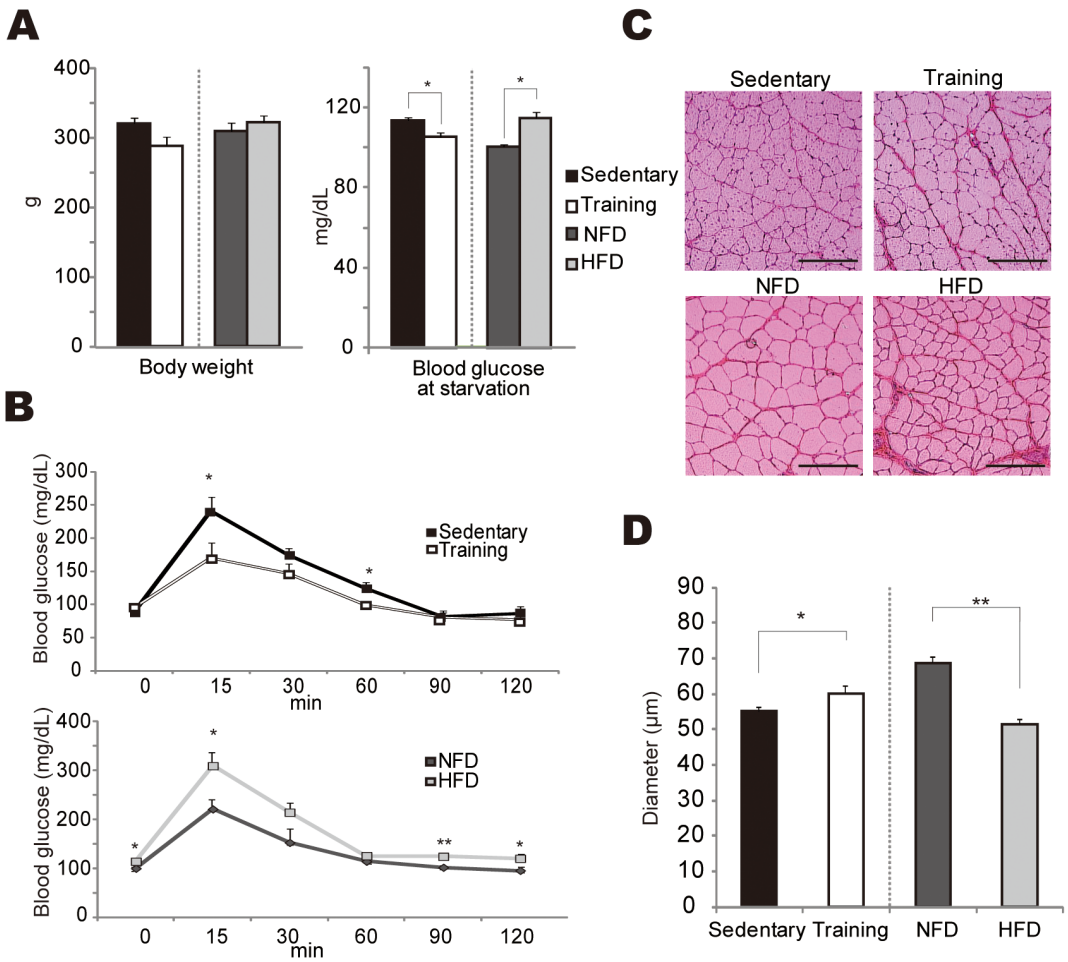


**Figure 1 | Characteristics of training and high-fat diet model.** (A) Comparison of body weight (left) and blood glucose level at starvation (right). (B) Glucose tolerance test results. (C) HE-stained sections of these four models. Scale bar: 200 μm. (D) The size of each myofiber was calculated and compared. Significant differences were determined by Student's t-test (n = 100).

Table 1 | Characteristics of the groups. The values represent means ± SE. * $p < 0.05$ compared to Sedentary rats. # $p < 0.05$ compared to rats fed a normal diet

| | Wistar rats 10 weeks | | Wistar rats 16 weeks | |
|---|---|---|---|---|
| | Sedentary | Training | Normal-fat diet | High-fat diet |
| Glucose | 113.6 ± 1.3 | 105.67 ± 2.02* | 100.33 ± 2.84 | 114.66 ± 3.18# |
| Body weight | 361.66 ± 7.75 | 324.33 ± 16.3 | 349.3 ± 13.62 | 362.66 ± 11.85 |

the value of area under the curve (AUC) of the Training group was significantly lower than that of the Sedentary group (Table 2). On the other hand, blood glucose levels in HFD rats were significantly higher those found in NFD rats at 15, 90, and 120 min after glucose injection (Fig. 1B), and the value of AUC of HFD was significantly higher than that of NFD (Table 2). Interestingly, the diameters of the minor axes of fibers in the Extensor digitorum longus (EDL) muscles were longer in the Training rats than in the Sedentary rats (Fig. 1C and 1D). In contrast, the muscle fiber diameter of HFD rats was shorter than that of the NFD rats (Fig. 1C and 1D). These observations indicate an anabolic effect of chronic exercise in the Training rats and an amyotrophic effect in the HFD rats. Moreover, the measurement of glucose transport *in vitro* showed significantly higher insulin sensitivity in Training rats, although the amount of insulin did not change (Fig. S1). It has been well demonstrated that chronic exercise and high-fat diet provide enhanced and diminished insulin sensitivity in skeletal muscle, respectively. Therefore, the insulin-sensitive model (Training) and the insulin-resistant model (HFD) are comparable for evaluating the roles of lipid profiles in skeletal muscle.

**Lipid analyses by thin-layer chromatography.** To identify and compare the lipid patterns of each pair, we separated these lipids by TLC. Figure 2A shows the thin-layer chromatograms of the extracted lipids. Phosphatidyletanolamine (PE), Phosphatidylinositol (PI), Phosphatodylserine (PS), Phosphatidylcholine (PC), and Sphingomyelin (SM) were detected with phospholipid separation. As shown in Figure 2A, there was a significant difference in the amount of SM, a precursor of ceramide, between the Sedentary and Training groups ($p < 0.05$), whereas there were no such differences between the NFD and HFD groups in any of the lipid classes.

TAG and DAG were also detected with neutral lipid separation. As shown in Figure 2B, there was a tendency toward decreased TAG levels in the Training group and increased levels in the HFD group. However, in terms of the total amounts, there was no significant difference between each pair.

**Visualization of lipids by imaging mass spectrometry.** We performed IMS-based histological examinations to reveal the characteristic lipid peaks in muscle tissues. Figure 3A represents ion images detected in positive-ion mode. In the present study, we focused on PC molecular species, and confirmed their localization[30]. Since the molecules are ionized as $[M + H]^+$, $[M + Na]^+$, and $[M + K]^+$, it was difficult to identify the molecules merely by comparing their molecular masses[13]. Therefore, we undertook a tandem mass spectrometric analysis to identify the molecules. First, we used each lipid standard to verify the fragmentation patterns, and compared tissue-derived tandem mass spectra with these patterns. In tandem mass spectrometric analyses, we could observe the fragment ions relating to their polar heads, adduct ions, and fatty acids. Representative tandem mass spectra of each lipid standard are shown in Figure S2. As shown in Table 3, this analysis revealed the existence of PC (diacyl-16 : 0/18 : 2), PC (diacyl-16 : 0/18 : 1), PC (diacyl-38 : 6), PC (diacyl-16 : 0/20 : 4), PC (diacyl-18 : 1/18 : 2), PC (diacyl-18 : 1/20 : 4), PC (diacyl-18 : 2/20 : 4), PC (diacyl-18 : 1/20 : 4), PC (diacyl-18 : 0/20 : 4), and PC (diacyl-18 : 2/22 : 6). As shown in Figure 3A, the ion images of all PC molecular species showed similar patterns. These distributions were ubiquitous in the EDL muscles (Fig. S3). A comparison of the Sedentary and Training rats revealed no significant differences in terms of the amount or localization of PC, which was in keeping with the TLC results. Meanwhile, a comparison of NFD and HFD rats demonstrated that levels of PC (diacyl-16 : 0/18 : 2) decreased moderately in HFD rats. The same tendency was observed in the case of PC (diacyl-18 : 2/22 : 6). Interestingly, levels of arachidonic acid (AA)-containing PCs, namely, PC (diacyl-16 : 0/20 : 4), PC (diacyl-18 : 2/20 : 4), PC (diacyl-18 : 1/20 : 4), and PC (diacyl-18 : 0/20 : 4), were all increased in HFD rats compared to NFD rats. To verify these compositional changes, linoleic acid (LA) and mono-unsaturated fatty acid (MUFA)-containing, AA-containing, and docosahexanoic acid (DHA)-containing PC were categorized (Fig. 3B). The lipid ratios in Sedentary and Training rats did not change (differences within 5%). Between NFD and HFD rats, the percentages of PC containing AA were dramatically increased in HFD rats. On the other hand, LA- and MUFA-containing PC levels were decreased in HFD rats, while DHA-containing PC amounts did not differ. This finding demonstrated that HFD-induced lipid compositional changes occur at the molecular-species level. The compositional lipid content of PUFA is higher in normal-fat food compared to high-fat food. Therefore this fatty acid ratio was not correlated to food consumption.

Figure 3C shows the IMS results in negative-ion mode. Only $[M - H]^-$ ions were detected in this mode. The ions were confirmed as PE (diacyl-16 : 0/22 : 6), PE (diacyl-18 : 0/20 : 4), PE (diacyl-18 : 0/22 : 6), PE (diacyl-18 : 0/22 : 6), and PI (diacyl-18 : 0/20 : 4), respectively. In the comparison of Sedentary and Training rats, ion intensities were found to be similar, and the ratio of DHA-containing and AA-containing PC did not differ (Fig. 3C and 3D). In the comparison of NFD and HFD rats, the same tendency was observed in the positive-ion mode; levels of AA-containing PE and PI were increased in HFD compared to NFD rats (Fig. 3C). Figure 3D shows circle graphs of PE composition, and reveals that AA-containing PEs were increased in HFD compared to NFD rats.

**Relative quantification of molecular species by TLC-Blot-MALDI-IMS.** In the PC bands, we focused on four major molecular species and performed quantitative analyses by TLC-Blot-MALDI-IMS. Interestingly, PC (diacyl-16 : 0/18 : 2) and PC (diacyl-18 : 0/22 : 6) were increased in the Training group compared to the Sedentary group, with significant differences observed ($p < 0.05$ and $p < 0.01$, respectively) (Fig. 4A). In the comparison of NFD and HFD rats, the ion images of AA-containing PC (diacyl-18 : 0/20 : 4) showed

Table 2 | The values of area under the curve (AUC) of glucose tolerance test. The values represent means ± SE. * $p < 0.05$ compared to Sedentary rats. # $p < 0.05$ compared to rats fed a normal diet

| | Wistar rats 9 weeks | | Wistar rats 16 weeks | |
|---|---|---|---|---|
| | Sedentary | Training | Normal-fat diet | High-fat diet |
| AUC | 15710 ± 522 | 13078 ± 975* | 14925 ± 919 | 20400 ± 879# |

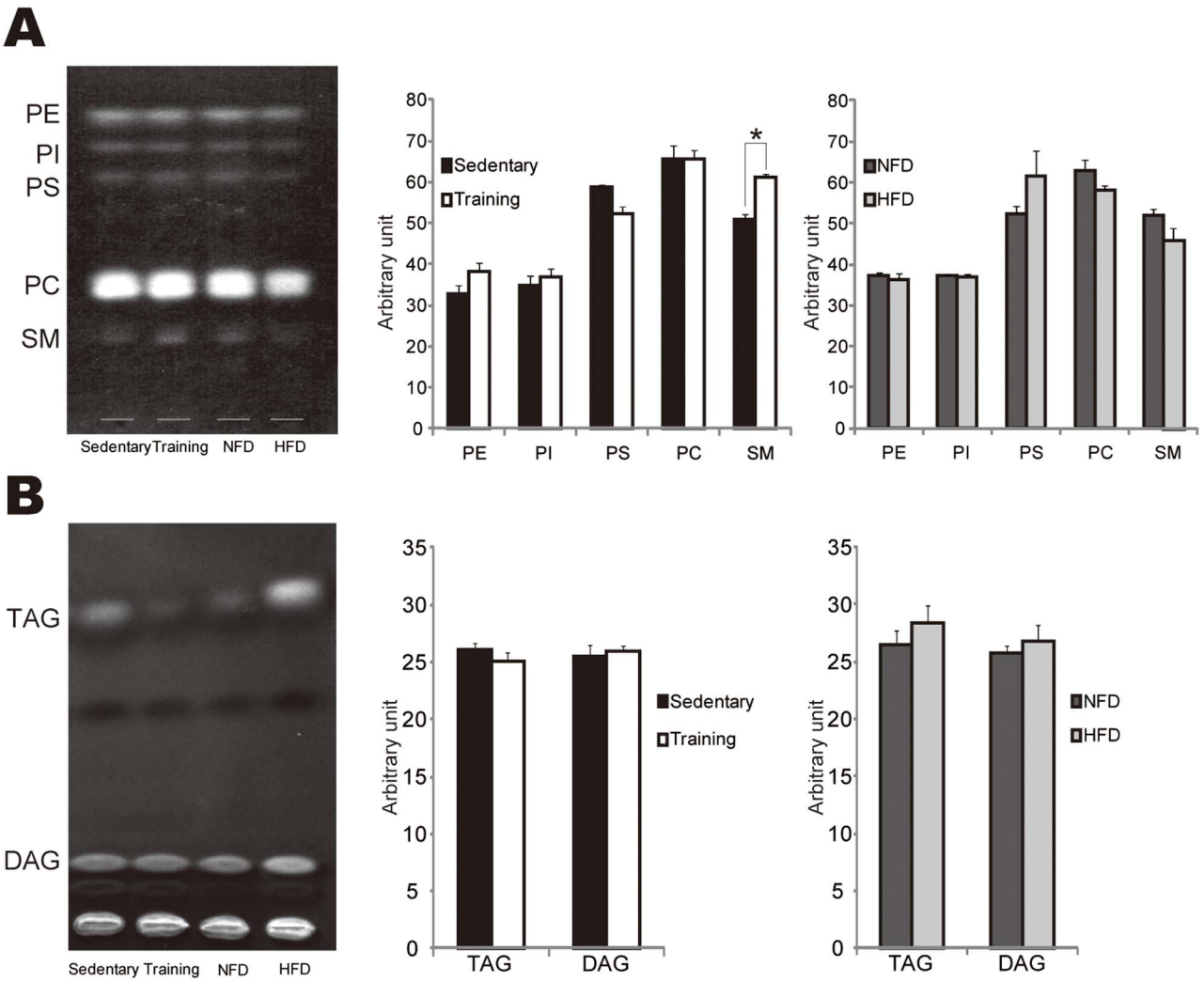


**Figure 2 | Thin-layer chromatography results.** (A) Phospholipid separation results indicated the PE, PI, PS, PC, and SM amounts of these models. Statistical analyses were performed. (B) Neutral lipid separation results indicated the DAG and TAG amounts of these models. No differences were found.

significantly higher levels in HFD than in NFD rats ($p < 0.05$) (Fig. 4A). On the other hand, PC (diacyl-16 : 0/18 : 2) levels were lower in HFD rats ($p < 0.05$) (Fig. 4A). The merged-ion images of three molecular species (Red, [diacyl-18 : 0/22 : 6]; Green, [diacyl-18 : 0/20 : 4]; and Blue, [diacyl-16 : 0/18 : 2]) demonstrated that compositional changes at the molecular-species level occurred in each pair.

As shown in Figure 4B, the SM bands were also analyzed quantitatively by TLC-Blot-MALDI-IMS. According to our results, abundant molecular species - namely, SM (d18 : 1/16 : 0) and SM (d18 : 1/18 : 0) - increased in the Training group; this was the same as the result obtained by TLC analysis. On the other hand, significantly higher levels of the long-chain fatty acids containing SMs, SM (d18 : 1/24 : 1) and SM (d18 : 1/24 : 0), were seen in HFD rats than in NFD rats. This result was first obtained by TLC-Blot-MALDI-IMS analyses.

We employed the same scheme for the TAG analysis, in which we detected eight molecular species: TAG (16 : 0/18 : 2/18 : 3), TAG (16 : 0/18 : 1/18 : 3), TAG (16 : 0/18 : 2/18 : 1), TAG (16 : 0/18 : 1/18 : 1), TAG (54 : 2), TAG (54 : 1), TAG (54 : 0), and TAG (16 : 0/20 : 3/18 : 1). However, no significant differences were found among species (data not shown).

## Discussion

The hypertrophic features of muscle fibers and the decreased blood glucose levels clearly revealed that the rats subjected to chronic exercise were well trained (Fig. 1). Additionally, in GTT test, the value of AUC was significantly lower in the Training group compared with that of the Sedentary group, while insulin stimulated glucose transport in EDL muscle was significantly higher in Training group. This suggested that our Training models represented higher insulin sensitivity in their muscle tissues. Atrophy is well known to be associated with the lower motor activity levels induced by obesity. As shown in Figure 1, the muscle fibers of HFD rats displayed this typical feature, and the GTT results showed that HFD rats had impaired glucose tolerance and increased blood glucose levels at starvation. These data confirmed that our HFD model represented insulin-resistant and moderate obesity. Because skeletal muscle serves as the major site of insulin-stimulated glucose clearance after a meal, it is reasonable to infer that abnormal lipid accumulation in this specific tissue type might play a key role in insulin sensitivity and/or resistance. Although there is substantial variety among previous observation protocols, we noted that there had not yet been a report on phospholipids at the molecular-species level, in spite of the abundance and importance of these lipid species. We selected the phenotype of moderate rather than severe obesity because we are interested in finding the lipid markers for the moderately obese condition.

Skeletal muscle consists of heterogeneous muscle fibers, which are typically classified into three fiber types: type I, type IIa, and type IIb. Since EDL muscle is relatively homogeneous, type II fibers predominate

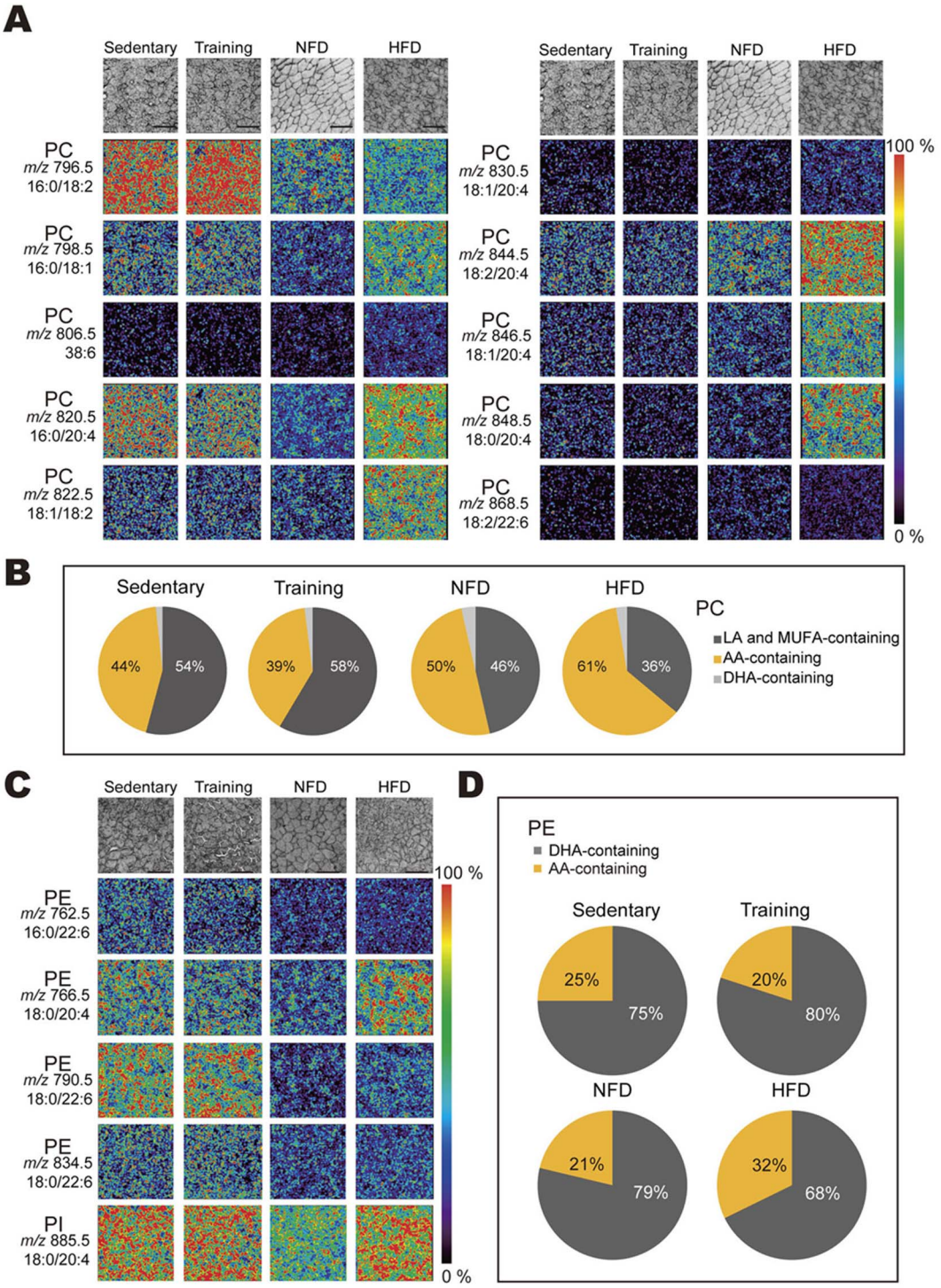


**Figure 3 | Imaging mass spectrometric analysis results.** (A) Positive-ion mode analyses reveal PC molecular species distribution. (B) Graph of IMS analyses of PC composition. (C) Negative-ion mode analyses reveal PE and PI molecular species distribution. (D) Graph of IMS analyses of PE composition. Scale bar is 200 μm. Color bars represent relative intensity values. These data were normalized with total ion current.

(Fig. S3). We selected EDL muscles to avoid regional variation of the muscle fibers, which enabled us to highlight that IMS is applicable for pathological experiments with small size biopsy muscle samples.

As shown in Figure 2, traditional TLC analyses showed a significant accumulation of SM only in the Training rats. This finding concurs with that of a previous study that revealed an increase in the total amount of SM in EDL from chronically trained mice[9]. Our present findings are also consistent with a previous study showing that chronic exercise reduced the amount of ceramides. Since SM is a precursor of ceramide produced by sphingomyelinase (SMase), the accumulation of SM might be associated with the exercise-induced decrease in ceramide. Ottestad and colleagues reported that an increase in muscle SM induced by a fish oil diet was related to a reduction in the risk of diabetes[31]. Therefore, a decrease in muscle ceramide and/or an increase in muscle SM may play a critical role in the upregulation of insulin activity in skeletal muscle. Additionally, another study hypothesized that a reduction in ceramides with chronic exercise was derived from the activation of SMase and serine

Table 3 | Detected molecules

| Lipid species | Observed *m/z* | Molecular structure | Adduct ion |
|---|---|---|---|
| PC | 796.5 | diacyl (16:0/18:2)* | $[M + K]^+$ |
| PC | 798.5 | diacyl (18:0/18:1)* | $[M + K]^+$ |
| PC | 806.5 | *diacyl (38:6)* | $[M + H]^+$ |
| PC | 810.5 | diacyl (18:0/20:4)* | $[M + H]^+$ |
| PC | 820.5 | diacyl (16:0/20:4)* | $[M + K]^+$ |
| PC | 822.5 | diacyl (18:1/18:2)* | $[M + K]^+$ |
| PC | 828.5 | diacyl (16:0/22:6)* | $[M + Na]^+$ |
| PC | 830.5 | diacyl (18:1/20:4)* | $[M + Na]^+$ |
| PC | 844.5 | diacyl (18:2/20:4)* | $[M + K]^+$ |
| PC | 846.5 | diacyl (18:1/20:4)* | $[M + K]^+$ |
| PC | 848.5 | diacyl (18:0/20:4)* | $[M + K]^+$ |
| PC | 856.5 | diacyl (18:0/22:6)* | $[M + Na]^+$ |
| PC | 868.5 | diacyl (18:2/22:6)* | $[M + K]^+$ |
| SM | 837.5 | d18:1/24:0* | $[M + Na]^+$ |
| SM | 835.5 | d18:1/24:1* | $[M + Na]^+$ |
| SM | 769.5 | d18:1/18:0* | $[M + K]^+$ |
| SM | 741.5 | d18:1/16:0* | $[M + K]^+$ |
| TAG | 875.7 | 16:0/18:2/18:3* | $[M + K]^+$ |
| TAG | 877.7 | 16:0/18:1/18:3* | $[M + K]^+$ |
| TAG | 879.7 | 16:0/18:2/18:1* | $[M + K]^+$ |
| TAG | 881.7 | 16:0/18:1/18:1* | $[M + Na]^+$ |
| TAG | 893.7 | *(54:2)* | *$[M + Na]^+$* |
| TAG | 895.7 | *(54:1)* | *$[M + Na]^+$* |
| TAG | 897.7 | *(54:0)* | *$[M + Na]^+$* |
| TAG | 921.7 | 16:0/20:3/18:1* | $[M + K]^+$ |
| PE | 762.5 | diacyl (16:0/22:6)* | $[M - H]^-$ |
| PE | 766.5 | diacyl (18:0/20:4)* | $[M - H]^-$ |
| PE | 790.5 | diacyl (18:0/22:6)* | $[M - H]^-$ |
| PE | 834.5 | diacyl (18:0/22:6)* | $[M - H]^-$ |
| PI | 885.5 | diacyl (18:0/20:4)* | $[M - H]^-$ |

*: identified by tandem mass spectrometric analysis.
*italic*: speculated molecules.

palmitoyl transferase[32]. Our study indicated that SMase might be a key enzyme in the metabolic change that Training rats showed with regards to SM accumulation. It is known that SM is an abundant molecule compared to ceramide, which might be a more sensitive marker of these changes. Interestingly, TLC-Blot-MALDI-IMS analyses revealed that a minor SM with a long-chain fatty acid, SM (d18:1/24:0), and SM (d18:1/24:1), which showed higher Relative-to-front values compared to SM (d18:1/16:0), were specifically increased in HFD rats, although the SM bands looked the same in the NFD and HFD rats. Consistent with our results, a previous report demonstrated that an HFD increased C24:1 containing ceramide[8]. Ceramide synthases have 6 isoforms, and ceramide synthase 2 (CerS2) has been reported to be specific for long-chain fatty acid residues (C22-C24)[33]. We assumed that CerS2 is also a key enzyme in HFD-induced metabolic changes in skeletal muscle.

Other phospholipids—namely, PC, PE, PI, and PS—were not found to differ in terms of total amounts when the groups were analyzed by TLC. We next conducted IMS analyses to detect distinct molecular species in muscle, because IMS is a screening method that enables verification of multiple molecular ions within small specimens. We selected 25 μm as the laser diameter. The mean diameter of each muscle fiber studied was around 50–65 μm (Fig. 1D); hence, a resolution of 25 μm was sufficient to detect each fiber-specific lipid.

In positive-ion mode, we focused on the most abundant lipid, PC. We found 10 molecular species of PC and confirmed their localizations. These localizations did not differ from each other; the signals were clearly spotted, which is a result of the particular features of the muscle fibers. It has previously been shown that the MALDI-IMS compositional ratio reflects the relative quantitative results followed by LC-ESI-MS analyses[34]. We therefore categorized the detected PCs into three groups: LA- and MUFA-containing, AA-containing, and DHA-containing PCs. In a comparison of the Sedentary and Training groups, no significant difference was detected in any of the molecular species. On the other hand, the comparison of NFD and HFD rats showed significant differences in the levels of certain molecular species. For example, the compositional ratio of AA-containing PCs was higher in HFD (61%) than in NFD rats (50%). Meanwhile, the compositional ratios of LA- and MUFA-containing PCs were reduced in HFD rats (Fig. 3B).

TLC-Blot-MALDI-IMS can be used for relative quantitative analyses with high reproducibility. This approach enables the visualization of each molecular species on a TLC plate, and thereby permits relative quantification among samples at the molecular-species level. We analyzed PC bands and constructed four major ion images (Fig. 4A). A merged image of these ions is also shown. As a result, AA-containing PC was detected predominantly in HFD, and Training rats exhibited higher amounts of PC (diacyl-18:0/22:6) and PC (diacyl-16:0/18:2) compared to Sedentary rats, with the results showing significant differences. The LA-containing PC (diacyl-16:0/18:2), exhibited the highest oxidation efficiency, and one report has noted that levels of this PC were increased in tumor tissue[35]. We speculated that the accumulation of this molecular species could act as an antioxidant; that is, Training rats could strengthen the antioxidant effects of muscles. Moreover, the result showing that levels of DHA-containing PC were increased in Training rats was expected in light of a previous finding that DHA supplementation altered the lipidomic profile and reduced diabetes risk[31]. It was also a unique finding that LA and AA showed comparable differences in HFD rats, even though LA and AA belong to the same omega 6 fatty acid group.

In negative-ion mode, we visualized PE and PI localization using IMS (Fig. 3C). Comparative analyses of the compositions of PE molecular species showed that the population of AA-containing PE was also increased in HFD rats (Fig. 3D). It is thought that AA is an important factor in skeletal muscle cell growth via a COX-2−dependent pathway[36]; in turn, AA then promotes skeletal muscle cell differentiation[37]. In addition, since AA is an inflammation-associated lipid mediator, it is reasonable to infer that AA-containing phospholipids accumulated in HFD rats, which exhibited inflammation in their atrophic muscles. We thus concluded that the accumulation of AA-containing PC, PE, and PI is associated with obesity.

The amounts of DAG and TAG did not differ in our models. These discrepancies might be due to differences in the duration of exercise training sessions and/or the type of exercise employed; one previous report noted that 6 weeks of training had no effect on neutral lipid amounts[38]. However, we used a short treatment period because we wanted to identify more sensitive biomarkers than TAG. As regards the EDL muscle we used for the HFD experiment, it can be difficult to detect an accumulation of lipids in this type of muscle[8]; TAG accumulation has been reported in other muscle types, such as soleus and gastrocnemius, which consist of type I fibers[7]. We realize that further investigation utilizing these muscles is needed.

It is known that the fatty acid remodeling of phospholipids can alter lipid metabolism, and that such alterations have been associated with a reduction in diabetes risk[31]. To the best of our knowledge, the present study is the first to demonstrate the effects of chronic exercise training and HFD on the rearrangement of phospholipid molecular species in skeletal muscle. Our results revealed chronic exercise-induced and HFD-induced lipids, which might be related to insulin sensitivity and resistance, respectively. Our findings suggest that the generally observed hypoinsulinemia induced by chronic exercise effectively arranges phospholipid composition and might be related to cell permeability or receptor stability, and/or to TAG droplet accumulation. We also found that our methodology could be successfully applied to small-sized specimens from biopsy samples. Further investigations are expected to elucidate the mechanisms underlying the effects of these specific lipid species on muscle function.

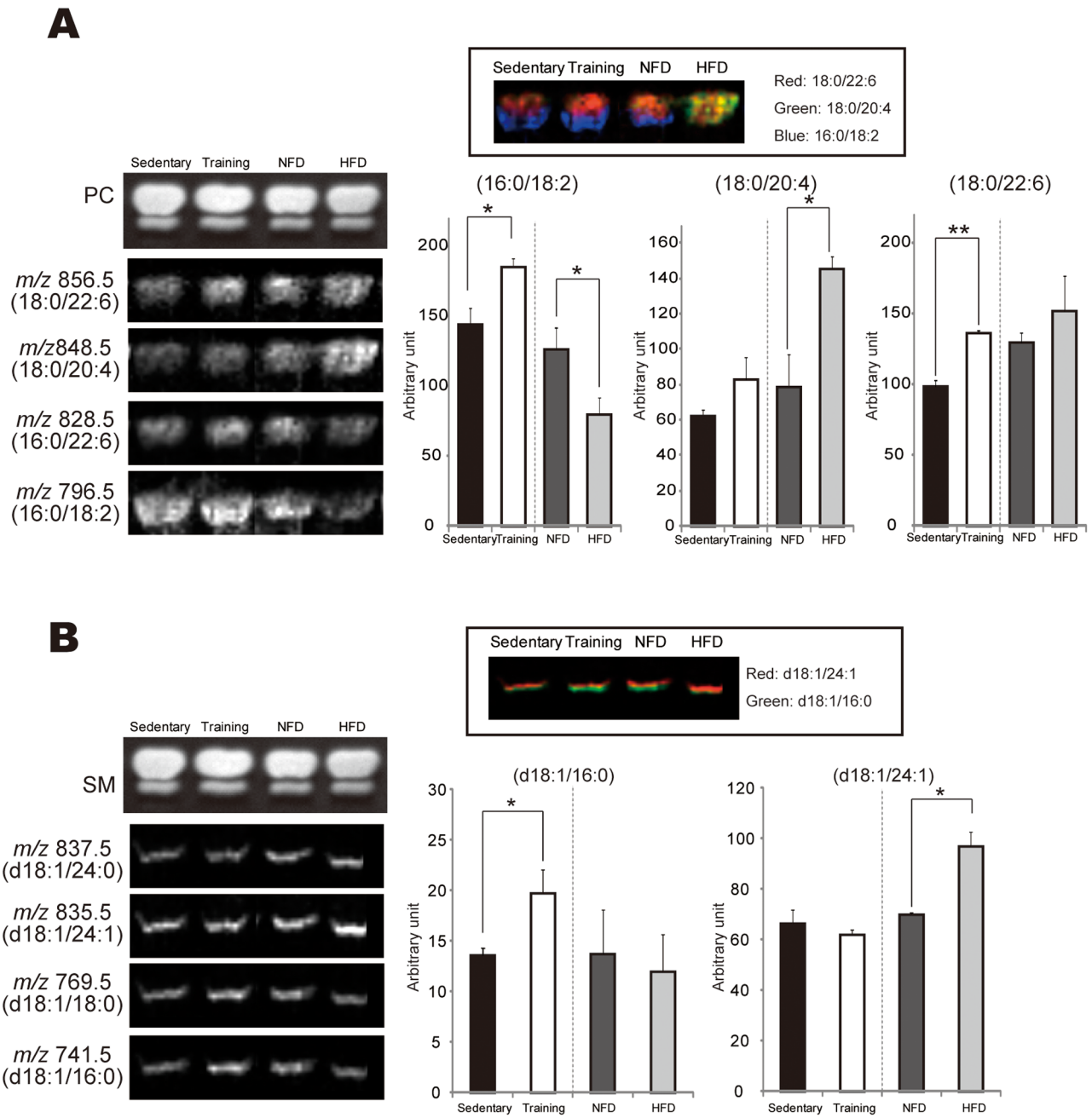


**Figure 4 | TLC-Blot-MALDI IMS analysis results.** (A) Relative quantification of PC molecular species. The visible TLC bands looks equal, but the compositional ratios of these molecular species differed between Sedentary and Training rats and between NFD and HFD rats. The ion images of *m/z* 796.5, 848.5, and 856.5 were merged. (B) Relative quantification of SM molecular species. The ion images of *m/z* 741.5 and 837.5 were merged. The measurement area of PC and SM were cut before experiments and analyzed the all area of visualized bands by primuline reagent. Full-length blots are presented in Supplementary Figure 4.

## Methods

**Materials.** Two matrices, 2, 5-dihydroxybenzoic acid (DHB) and 2, 5-dihydroxyacetophenone (DHAP), were purchased from Bruker Daltonics (Bremen, Germany). Methanol, ethanol, and ultra pure water (Wako Pure Chemical Industries, Osaka, Japan) were used for the preparation of all buffers and solvents. All chemicals used in this study were of the highest purity available.

**Rats, diets, and exercise training.** The care and use of these laboratory animals were in accordance with the Experimental Animal Committee of Tokyo Metropolitan University and followed the Guidelines for the Proper Conduct of Animal Experiments established by the Science Council of Japan. The experimental protocol was approved by the Experimental Animal Committee of Tokyo Metropolitan University. Three-week-old male Wistar rats, purchased from Japan CLEA with an initial body weight of approximately 120 g, were housed 2 in a cage in a temperature-controlled room with a 12-hour light-dark cycle. EDL muscles were used for all analyses, and all experiments were performed in biological replicate (n = 6–7).

*Exercise training.* The animals were randomly assigned to one of two experimental groups: sedentary control (Sedentary) and Training groups. Prior to the chronic exercise protocol, the Training rats were habituated to treadmill running for 15 min from 0 to 15 m/min for 5 days. After adaptation, the Training group was subjected to chronic exercise on a treadmill for 60 min at 25 m/min, 5 days per week, for 6 weeks. When the Training rats exercised, the Sedentary rats were placed beside the treadmill and exposed to the same environment, but did not run. The Training rats were sacrificed 36 hours or more after the last exercise session.

*Diet control.* We assigned the 3-week-old male Wistar rats to a normal-diet control (NFD) group or a HFD group for the 12-week duration of the study. The HFD was formulated to provide 60% of total energy from lard, D12492; Research Diets, Inc. (New Brunswick, NJ). The compositional lipid contents of poly-unsaturated were

47.2 % and 32% in NFD and HFD, respectively. After 16 hours' starvation, the rats in both groups were sacrificed and their EDL muscles were dissected.

**Glucose tolerance test.** Blood glucose levels were measured from tail blood using OneTouch® Ultra® (LifeScan, Inc., Milpitas, CA). For the glucose tolerance test (GTT), the rats were fasted overnight. The GTT was performed in a quiet room, and handling was minimized during the procedure. The rats were measured blood glucose level for basal condition (time point, 0 min), and weighted to calculate glucose dosage based on body weight for the GTT. Then, glucose was injected intraperitoneally (2 mg/g body weight). Blood samples were obtained from the tail veins at 15, 30, 60, 90, and 120 min after injection.

**Lipid analysis.** Total lipids were extracted from EDL muscle samples with chloroform/methanol (2 : 1, v/v). Lipid fractions were extracted by the Bligh and Dyer method as described previously[39]. Equal amounts of the extract were manually applied on silica gel 60 high-performance thin-layer chromatography (HPTLC) plates (Merck, Darmstadt, Germany). The plates were developed with a solvent system consisting of methyl acetate/1-propanol/chloroform/methanol/0.25% aqueous potassium chloride (25 : 25 : 25 : 10 : 9, v/v/v/v/v) for phospholipids, whereas for TAG separation, the developing solvent was composed of n-hexane/diethyl ether/acetic acid (80/30/1, v/v/v). These chromatograms were sprayed with 0.005% (w/v) primuline reagent, and lipid bands were visualized under ultraviolet light at 302 nm. The relative densities of each lipid were quantitatively determined by Image J software (http://rsbweb.nih.gov/ij/). The developed TLC plates were transferred to a PVDF membrane by the TLC-Blot method as described previously[25]. Transferred PVDF membranes were attached to the MALDI target plate, and mass spectrometric analyses were performed.

**Histochemical staining.** Muscles were frozen in 2-methylbuthan and liquid nitrogen and stored at −80°C without fixation. Sections were prepared as described previously[19] but with slight modifications. Consecutive 10-μm sections were cut using a cryostat (CM 1850; Leica Microsystems, Wetzlar, Germany). The serial sections were mounted onto MAS-coated slides (Matsunami, Osaka, Japan) for histochemical staining, and indium tin oxide (ITO)-coated glass slides (Bruker Daltonics) for imaging mass spectrometry. For morphological observation, serial sections were subjected to hematoxylin-eosin (HE) staining and immunohistochemical staining with monoclonal anti-myosin (skeletal, fast) antibody (Sigma-Aldrich, Japan).

**Imaging mass spectrometry.** IMS analyses were performed by an atmospheric pressure ion-source mass spectrometer with a laser frequency of 1000 Hz (Mass Microscope; Shimadzu, Kyoto, Japan). All analyses were performed in the positive-ion mode within the mass ranges of *m/z* 600–1000 with DHB of 50 mg/mL, and in the negative-ion mode within the mass ranges of *m/z* 200–1000 with DHAP of 20 mg/mL as matrix. A 10-μm raster width was set to generate images of the muscles. The ion images were constructed using BioMap software (Novartis, Basel, Switzerland). All spectra were normalized by total ion current. The MS parameters were set to obtain the highest sensitivity. For TLC-Blot-MALDI-IMS, we used a QSTAR Elite high-performance, hybrid quadrupole time-of-flight mass spectrometer (Applied Biosystems, Foster City, CA). The laser irradiated 500 times per position on the PVDF membrane. All pixels in the images were 400 μm.

**Tandem mass spectrometry.** Tandem mass spectrometric analysis was performed using a QSTAR Elite according to a previously described procedure[13].

**Data analysis.** Data are presented as means ± SE. Statistical analysis was performed using StatView 5.0 (SAS Institute, Tokyo, Japan).


1. Watt, M. J. & Hoy, A. J. Lipid metabolism in skeletal muscle: generation of adaptive and maladaptive intracellular signals for cellular function. *Am J Physiol Endocrinol Metab* **302**, E1315–1328 (2012).
2. Pan, D. A. *et al.* Skeletal muscle triglyceride levels are inversely related to insulin action. *Diabetes* **46**, 983–988 (1997).
3. Muoio, D. M. Revisiting the connection between intramyocellular lipids and insulin resistance: a long and winding road. *Diabetologia* **55**, 2551–2554 (2012).
4. Samuel, V. T. & Shulman, G. I. Mechanisms for insulin resistance: common threads and missing links. *Cell* **148**, 852–871 (2012).
5. Liu, L. *et al.* Upregulation of myocellular DGAT1 augments triglyceride synthesis in skeletal muscle and protects against fat-induced insulin resistance. *J Clin Invest* **117**, 1679–1689 (2007).
6. Dube, J. J. *et al.* Exercise-induced alterations in intramyocellular lipids and insulin resistance: the athlete's paradox revisited. *Am J Physiol Endocrinol Metab* **294**, E882–888 (2008).
7. Turpin, S. M. *et al.* Examination of 'lipotoxicity' in skeletal muscle of high-fat fed and ob/ob mice. *J Physiol* **587**, 1593–1605 (2009).
8. Amati, F. *et al.* Skeletal muscle triglycerides, diacylglycerols, and ceramides in insulin resistance: another paradox in endurance-trained athletes? *Diabetes* **60**, 2588–2597 (2011).
9. Gorski, J., Zendzian-Piotrowska, M., de Jong, Y. F., Niklinska, W. & Glatz, J. F. Effect of endurance training on the phospholipid content of skeletal muscles in the rat. *Eur J Appl Physiol Occup Physiol* **79**, 421–425 (1999).
10. Goto-Inoue, N., Hayasaka, T., Zaima, N. & Setou, M. Imaging mass spectrometry for lipidomics. *Biochim Biophys Acta* **1811**, 961–969 (2011).
11. Chakravarthy, M. V. *et al.* Identification of a physiologically relevant endogenous ligand for PPARalpha in liver. *Cell* **138**, 476–488 (2009).
12. Tsuchiya, M. *et al.* Chronic exercise enhances insulin secretion ability of pancreatic islets without change in insulin content in non-diabetic rats. *Biochem Biophys Res Commun* **430**, 676–682 (2012).
13. Hayasaka, T., Goto-Inoue, N., Zaima, N., Kimura, Y. & Setou, M. Organ-specific distributions of lysophosphatidylcholine and triacylglycerol in mouse embryo. *Lipids* **44**, 837–848 (2009).
14. Murphy, R. C., Hankin, J. A. & Barkley, R. M. Imaging of lipid species by MALDI mass spectrometry. *J Lipid Res* **50 Suppl**, S317–322 (2009).
15. Touboul, D. *et al.* Changes of phospholipid composition within the dystrophic muscle by matrix-assisted laser desorption/ionization mass spectrometry and mass spectrometry imaging. *Eur J Mass Spectrom (Chichester, Eng)* **10**, 657–664 (2004).
16. Zaima, N., Hayasaka, T., Goto-Inoue, N. & Setou, M. Imaging of metabolites by MALDI mass spectrometry. *J Oleo Sci* **58**, 415–419 (2009).
17. Colsch, B. & Woods, A. S. Localization and imaging of sialylated glycosphingolipids in brain tissue sections by MALDI mass spectrometry. *Glycobiology* **20**, 661–667 (2010).
18. Goto-Inoue, N. *et al.* Imaging mass spectrometry visualizes ceramides and the pathogenesis of dorfman-chanarin syndrome due to ceramide metabolic abnormality in the skin. *PLoS One* **7**, e49519 (2012).
19. Goto-Inoue, N., Hayasaka, T., Zaima, N. & Setou, M. The specific localization of seminolipid molecular species on mouse testis during testicular maturation revealed by imaging mass spectrometry. *Glycobiology* **19**, 950–957 (2009).
20. Stoeckli, M., Chaurand, P., Hallahan, D. E. & Caprioli, R. M. Imaging mass spectrometry: a new technology for the analysis of protein expression in mammalian tissues. *Nat Med* **7**, 493–496 (2001).
21. Yao, I., Sugiura, Y., Matsumoto, M. & Setou, M. In situ proteomics with imaging mass spectrometry and principal component analysis in the Scrapper-knockout mouse brain. *Proteomics* **8**, 3692–3701 (2008).
22. Goto-Inoue, N., Setou, M. & Zaima, N. Visualization of spatial distribution of gamma-aminobutyric acid in eggplant (Solanum melongena) by matrix-assisted laser desorption/ionization imaging mass spectrometry. *Anal Sci* **26**, 821–825 (2010).
23. Zaima, N., Goto-Inoue, N., Hayasaka, T. & Setou, M. Application of imaging mass spectrometry for the analysis of Oryza sativa rice. *Rapid Commun Mass Spectrom* **24**, 2723–2729 (2010).
24. Hu, C. *et al.* Lipidomics analysis reveals efficient storage of hepatic triacylglycerides enriched in unsaturated fatty acids after one bout of exercise in mice. *PLoS One* **5**, e13318 (2010).
25. Goto-Inoue, N. *et al.* High-sensitivity analysis of glycosphingolipids by matrix-assisted laser desorption/ionization quadrupole ion trap time-of-flight imaging mass spectrometry on transfer membranes. *J Chromatogr B Analyt Technol Biomed Life Sci* **870**, 74–83 (2008).
26. Goto-Inoue, N., Hayasaka, T., Taki, T., Gonzalez, T. V. & Setou, M. A new lipidomics approach by thin-layer chromatography-blot-matrix-assisted laser desorption/ionization imaging mass spectrometry for analyzing detailed patterns of phospholipid molecular species. *J Chromatogr A* **1216**, 7096–7101 (2009).
27. Taki, T. & Ishikawa, D. TLC blotting: application to microscale analysis of lipids and as a new approach to lipid-protein interaction. *Anal Biochem* **251**, 135–143 (1997).
28. Petkovic, M. *et al.* Detection of individual phospholipids in lipid mixtures by matrix-assisted laser desorption/ionization time-of-flight mass spectrometry: phosphatidylcholine prevents the detection of further species. *Anal Biochem* **289**, 202–216 (2001).
29. Zaima, N., Goto-Inoue, N., Adachi, K. & Setou, M. Selective analysis of lipids by thin-layer chromatography blot matrix-assisted laser desorption/ionization imaging mass spectrometry. *J Oleo Sci* **60**, 93–98 (2011).
30. Goto-Inoue, N. *et al.* Visualization of dynamic change in contraction-induced lipid composition in mouse skeletal muscle by matrix-assisted laser desorption/ionization imaging mass spectrometry. *Anal Bioanal Chem* **403**, 1863–1871 (2012).
31. Ottestad, I. *et al.* Fish oil supplementation alters the plasma lipidomic profile and increases long-chain PUFAs of phospholipids and triglycerides in healthy subjects. *PLoS One* **7**, e42550 (2012).
32. Blachnio-Zabielska, A., Zabielski, P., Baranowski, M. & Gorski, J. Aerobic training in rats increases skeletal muscle sphingomyelinase and serine palmitoyltransferase activity, while decreasing ceramidase activity. *Lipids* **46**, 229–238 (2011).
33. Imgrund, S. *et al.* Adult ceramide synthase 2 (CERS2)-deficient mice exhibit myelin sheath defects, cerebellar degeneration, and hepatocarcinomas. *J Biol Chem* **284**, 33549–33560 (2009).
34. Yang, H. J., Sugiura, Y., Ikegami, K., Konishi, Y. & Setou, M. Axonal gradient of arachidonic acid-containing phosphatidylcholine and its dependence on actin dynamics. *J Biol Chem* **287**, 5290–5300 (2012).
35. Ishikawa, S. *et al.* Increased expression of phosphatidylcholine (16 : 0/18 : 1) and (16 : 0/18 : 2) in thyroid papillary cancer. *PLoS One* **7**, e48873 (2012).
36. Markworth, J. F. & Cameron-Smith, D. Arachidonic acid supplementation enhances in vitro skeletal muscle cell growth via a COX-2-dependent pathway. *Am J Physiol Cell Physiol* **304**, C56–67 (2013).

37. Briolay, A., Jaafar, R., Nemoz, G. & Bessueille, L. Myogenic differentiation and lipid-raft composition of L6 skeletal muscle cells are modulated by PUFAs. *Biochim Biophys Acta* **1828**, 602–613 (2012).
38. Sene-Fiorese, M. *et al.* Efficiency of intermittent exercise on adiposity and fatty liver in rats fed with high-fat diet. *Obesity (Silver Spring)* **16**, 2217–2222 (2008).
39. Bligh, E. G. & Dyer, W. J. A rapid method of total lipid extraction and purification. *Can J Biochem Physiol* **37**, 911–917 (1959).

## Acknowledgments

This work was supported by a grant-in-aid for Kiban C to N. G.-I., and by a grant-in-aid to N.L.F. from the Funding Program for World-Leading Innovative R&D in Science and Technology from the Council for Science and Technology Policy.

## Author contributions

N.G.-I. and N.L.F. designed the experiments, wrote the main manuscript text and prepared figures. A.I., Y.F., K.Y., S.O., Y.M. helped the experiments. M.S. supervised the experiment. All authors reviewed the manuscript.

## Additional information

**Supplementary information** accompanies this paper at http://www.nature.com/scientificreports

**Competing financial interests:** The authors declare no competing financial interests.

**How to cite this article:** Goto-Inoue, N. *et al.* Lipidomics analysis revealed the phospholipid compositional changes in muscle by chronic exercise and high-fat diet. *Sci. Rep.* **3**, 3267; DOI:10.1038/srep03267 (2013).